



ELSEVIER

Available at

www.ElsevierMathematics.com

POWERED BY SCIENCE @ DIRECT®

JOURNAL OF  
COMPUTATIONAL AND  
APPLIED MATHEMATICS

Journal of Computational and Applied Mathematics 161 (2003) 119–132

www.elsevier.com/locate/cam

# Semi-implicit finite volume scheme for image processing in 3D cylindrical geometry

Karol Mikula<sup>a,\*</sup>, Fiorella Sgallari<sup>b</sup>

<sup>a</sup>*Department of Mathematics, Slovak University of Technology, Radlinského 11, 813 68 Bratislava, Slovakia*

<sup>b</sup>*Department of Mathematics, University of Bologna, Piazza di Porta S. Donato 5, 40127 Bologna, Italy*

Received 10 January 2003; received in revised form 2 April 2003

## Abstract

Nowadays, 3D echocardiography is a well-known technique in medical diagnosis. Inexpensive echocardiographic acquisition devices are applied to scan 2D slices rotated along a prescribed direction. Then the discrete 3D image information is given on a cylindrical grid. Usually, this original discrete image intensity function is interpolated to a uniform rectangular grid and then numerical schemes for 3D image processing operations (e.g. nonlinear smoothing) in the uniform rectangular geometry are used. However, due to the generally large amount of noise present in echocardiographic images, the interpolation step can yield undesirable results. In this paper, we avoid this step and suggest a 3D finite volume method for image selective smoothing directly in the cylindrical image geometry. Specifically, we study a semi-implicit 3D cylindrical finite volume scheme for solving a Perona-Malik-type nonlinear diffusion equation and apply the scheme to 3D cylindrical echocardiographic images. The  $L_\infty$ -stability and convergence of the scheme to the weak solution of the regularized Perona-Malik equation is proved.

© 2003 Elsevier B.V. All rights reserved.

*Keywords:* Partial differential equations; Nonlinear diffusion; Finite volume method; Semi-implicit scheme; Image processing; Cylindrical geometry; Echocardiography

## 1. Introduction

Since the end of the 1980s, nonlinear diffusion equations have been used for processing 2D and 3D images. After the pioneering work of Perona and Malik [17], who modified the linear heat equation [23,11] to a nonlinear diffusion equation, which preserves edges, there has been a great

\* Corresponding author.

E-mail addresses: mikula@vox.svf.stuba.sk (K. Mikula), sgallari@dm.unibo.it (F. Sgallari).

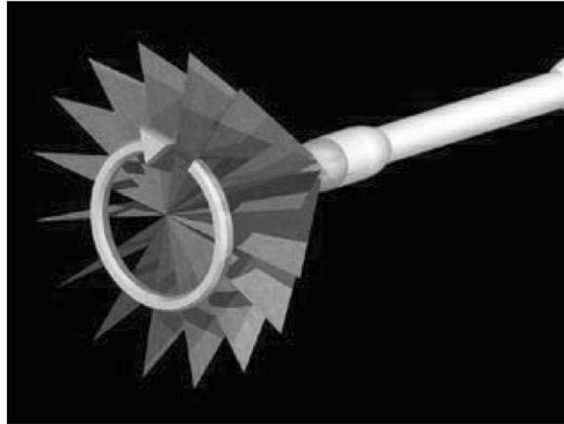


Fig. 1. The echocardiographic acquisition device.

deal of interest in the application and analysis of such equations [1]. One of the most important application is medical image processing.

For example, due to its noninvasive character and ability to view anatomical structures, 3D medical ultrasound (e.g. echocardiography) has become an important modality in diagnosis, assessment and management of a large number of diseases. Nevertheless, ultrasound imaging suffers from limitations that prevent its full potentiality. The inexpensive echocardiographic real-time acquisition devices now in common clinical use yield images with poor resolution and a large amount of noise [5,7]. Using a nonlinear diffusion equation of Perona-Malik-type [17] is computationally challenging. Our approach uses the structure of 2D slices acquired along nonaligned rotating planes by the echocardiographic acquisition device (see Figs. 1 and 2). We avoid the interpolation of very noisy data to obtain a regular cartesian lattice [2] and carry out image selective smoothing in the given discrete 3D cylindrical structure. Let us note that also more general 4D (3D+time) echocardiographic image anisotropic filtering [19] and 3D/4D segmentation models [14] can be realized in cylindrical geometry using ideas of this paper, allowing computational time gain, more detailed surface rendering and 3D volume analysis/display. This will be discussed in forthcoming work.

In this paper, we consider the following Perona-Malik-type nonlinear PDE [3] suggested by Catté et al. for image selective smoothing

$$u_t - \nabla \cdot (g(|\nabla G_\sigma * u|) \nabla u) = 0. \quad (1)$$

Here,  $u(t, x)$  is an unknown function defined in  $Q_T \equiv [0, T] \times \Omega$ , where  $I = [0, T]$  is the so-called scaling interval and  $\Omega$  is a cylindrical domain. Any horizontal cut of  $\Omega$  is shown in Fig. 3. Due to the natural image processing constraint to conserve a mass of the image intensity [20], Eq. (1) is accompanied by zero Neumann boundary condition

$$\frac{\partial u}{\partial \nu} = 0 \quad \text{on} \quad I \times \partial \Omega, \quad (2)$$

where  $\nu$  is the unit normal vector to the boundary of  $\Omega$ . The initial condition

$$u(0, x) = u^0(x) \quad \text{in} \quad \Omega \quad (3)$$

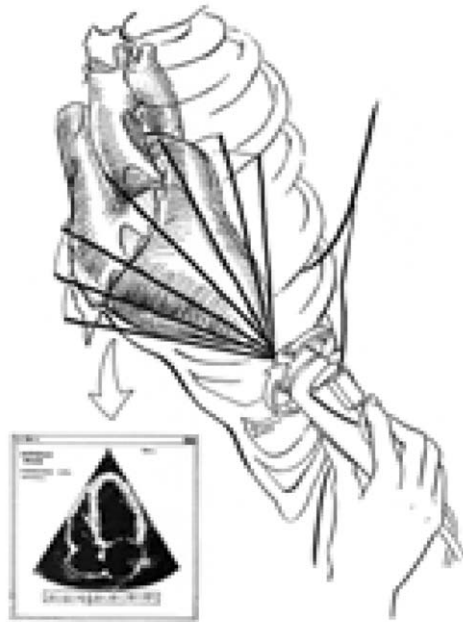


Fig. 2. A schematic picture of acquisition; original rotational data information given in discrete cuttings of cone is in every rotating plane just supplemented by black color to have rotating rectangular 2D slices which give together discrete 3D cylindrical geometry.

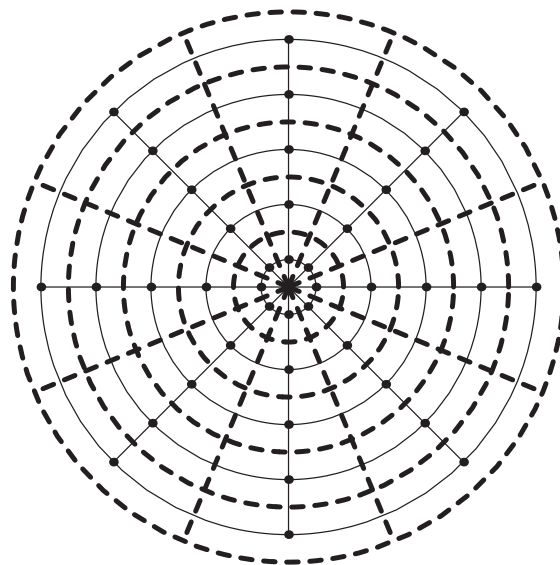


Fig. 3. The horizontal cut of finite volume cylindrical grid.

is given by the available contaminated image  $u^0$ . We assume that

$$g : \mathbb{R}_0^+ \rightarrow \mathbb{R}^+ \text{ is a nonincreasing function, } g(\sqrt{s}) \text{ is smooth,} \quad (4)$$

$$g(0) = 1, \quad \text{and} \quad g(s) \rightarrow 0 \text{ as } s \rightarrow \infty,$$

$$G_\sigma \in C^\infty(\mathbb{R}^d) \text{ is a smoothing kernel, e.g., the Gauss function,} \quad (5)$$

$$G_\sigma(x) \rightarrow \delta_x \text{ as } \sigma \rightarrow 0, \quad \delta_x \text{ is the Dirac function at the point } x,$$

$$u^0 \in L_\infty(\Omega), \quad (6)$$

and

$$\nabla G_\sigma * u = \int_{\mathbb{R}^d} \nabla G_\sigma(x - \xi) \tilde{u}(\xi) \, d\xi, \quad (7)$$

where  $\tilde{u}$  is an extension of  $u$  by 0 from  $\Omega$  to  $\mathbb{R}^3$ .

Eq. (1) represents a modification of the original Perona-Malik model [17,10]

$$u_t - \nabla \cdot (g(|\nabla u|) \nabla u) = 0, \quad (8)$$

also called *anisotropic diffusion* in the computer vision community. Perona and Malik introduced Eq. (8) in the context of image smoothing and edge enhancement. The equation selectively diffuses the image in the regions where the signal has small variance in intensity, but not in regions where the signal changes its intensity. This diffusion process is governed by the shape of the diffusion coefficient given by the function  $g$  in (4) and by its dependence on  $|\nabla u|$ , which is understood as an edge indicator [17]. Since  $g \rightarrow 0$  for large gradients, the diffusion is strongly slowed down at edges, while away from edges it provides averaging of pixel intensities as in the linear case. For practical choices of  $g$  (e.g.  $g(s) = 1/(1+s^2)$ ,  $g(s) = e^{-s^2}$ ), the original Perona-Malik equation behaves locally like the backward heat equation. Thus, in spite of its nonnegative diffusivity, the Perona-Malik model exhibits simultaneously forward and backward diffusion areas. As a consequence, the classical theory of existence and uniqueness does not apply anymore, and it seems to be unlikely that there exists a unique smooth solution [3,10]. Nevertheless, because of its visually impressive results, the Perona-Malik idea has triggered numerous modifications. By means of temporal or spatial regularization, nonlinear diffusion filters were proposed which are more robust against noise [3,4,15,21,22]. The nonlinear filter of Catté et al. in [3] is a well-investigate representative. These authors replace the diffusivity  $g(|\nabla u|)$  of the Perona-Malik model by  $g(|\nabla u_\sigma|)$  with  $u_\sigma := G_\sigma * u$  and established existence, uniqueness and regularity of the solution for  $\sigma > 0$ . Further improvements were achieved by anisotropic diffusion models which smooth preferently *along edges*. This may be accomplished by using a diffusion tensor instead of a scalar diffusivity or by convolving the image with anisotropic Gaussian [4,15,21,22].

In Section 2 we introduce semi-implicit finite volume scheme for solving regularized Perona-Malik equation (1) in 3D cylindrical geometry and prove its convergence to the weak solution of the problem. In Section 3 we present numerical experiments computed by the scheme especially in the case of 3D echocardiography.

## 2. The numerical method

Assume that there are  $l$  rotating 2D slices with  $m \times n$  discrete points, where  $m$  is the horizontal and  $n$  the vertical dimension, respectively. Usually  $m$  is even, i.e., the slices do not have common intersecting discrete point. We embed this discrete structure into the finite volume mesh in such a way that every discrete point is a *representative* inner “central” point of 3D finite volume. A horizontal cut of such a mesh is depicted in Fig. 3 for  $l = 4$  and  $m = 10$ . In the figure, the circular points represent the acquisition nodes, while dashed lines give the structure of our finite volumes around these points. In Fig. 3 one can also see a dual grid given by solid lines which connect the representative points of the finite volumes.

Let  $\mathcal{T}_h$  be such a finite volume mesh of  $\Omega$ . For every pair  $(p, q) \in \mathcal{T}_h^2$  with  $p \neq q$ , we denote their common interface by  $e_{pq}$ , i.e.,  $e_{pq} = \bar{p} \cap \bar{q}$ , which is supposed to be included in a hypersurface of  $\mathbb{R}^3$  not intersecting either  $p$  or  $q$ . In our case, a horizontal cut of  $e_{pq}$  is either a straight line or an arc. Let  $m(e_{pq})$  denote the measure of  $e_{pq}$ , and  $n_{pq}(x)$  the unit vector normal to  $e_{pq}$  at the point  $x \in e_{pq}$  oriented from  $p$  to  $q$ . We denote by  $\mathcal{E}$  the set of pairs of adjacent control volumes, defined by  $\mathcal{E} = \{(p, q) \in \mathcal{T}_h^2, p \neq q, m(e_{pq}) \neq 0\}$ . We also use the notation  $N(p) = \{q, (p, q) \in \mathcal{E}\}$ . Let  $x_p, p \in \mathcal{T}_h$  denote the representative point of the finite volume  $p$ ,  $\sigma_{pq}$  the co-edge of the interface  $e_{pq}$ , i.e., the part of the dual grid connecting  $x_p$  and  $x_q$  (this is again either a straight line or an arc) and  $x_{pq}$  the point of intersection of  $e_{pq}$  and  $\sigma_{pq}$ . Let  $\delta(p)$  denote the diameter of the control volume  $p$ ,  $m(p)$  the measure in  $\mathbb{R}^3$  of the control volume  $p$ ,  $\partial p$  its boundary and let  $h = \max_{p \in \mathcal{T}_h} \delta(p)$ .

In order to derive a discrete finite volume numerical method in cylindrical geometry, we start by the semi-discretization in scale of the problem given by (1). Choosing  $N \in \mathbb{N}$ , we obtain the length of the uniform discrete scale step  $k = T/N$ . We replace the scale derivative in (1) by a backward difference. The value of the nonlinear term of the equation is from the previous scale level while the linear terms are considered at the current scale level—this makes the method semi-implicit [9,8,20]. We obtain for every  $n = 1, \dots, N$  the equation

$$\frac{u^n - u^{n-1}}{k} - \nabla \cdot (g(|\nabla G_\sigma * u^{n-1}|) \nabla u^n) = 0 \tag{9}$$

for the (unknown) function  $u^n$ , which approximates the image intensity at the  $n$ th discrete scale step  $t_n = nk$ .

Let us denote by  $\bar{u}_p^n$  the representative value of  $u^n$  for the 3D finite volume  $p$ . In order to derive a spatial discretization, we integrate (9) over a finite volume  $p$

$$\int_p \frac{u^n - u^{n-1}}{k} dx = \int_p \nabla \cdot (g(|\nabla G_\sigma * u^{n-1}|) \nabla u^n) dx. \tag{10}$$

Using the divergence theorem on the right-hand side, we obtain

$$\begin{aligned} & \int_p \nabla \cdot (g(|\nabla G_\sigma * u^{n-1}|) \nabla u^n) dx \\ &= \int_{\partial p} g(|\nabla G_\sigma * u^{n-1}|) \frac{\partial u^n}{\partial \nu} ds = \sum_{q \in N(p)} \int_{e_{pq}} g(|\nabla G_\sigma * u^{n-1}|) \frac{\partial u^n}{\partial \nu} ds. \end{aligned}$$

Then, by means of  $\bar{u}_p^n$ , we approximate the normal derivative along the boundary of  $p$ , namely  $\partial u^n / \partial \nu \approx (\bar{u}_q^n - \bar{u}_p^n) / m(\sigma_{pq})$  along  $e_{pq}$ . The value of the diffusion coefficient along  $e_{pq}$  is approximated

by its value at the point  $x_{pq}$ . Since the dual grid and the boundary of finite volumes contain curvilinear parts, there is a difference between standard “polygonal” finite volume method described in [6,13] and the method presented in this paper. Our approach follows [16] - Section 4.6.2.

*A linear semi-implicit fully discrete finite volume scheme:* For each  $n = 1, \dots, N$ , we determine  $\bar{u}_p^n, p \in \mathcal{T}_h$ , that satisfies

$$\frac{m(p)}{k} \bar{u}_p^n + \sum_{q \in N(p)} g_{pq}^{\sigma, n-1} \frac{m(e_{pq})}{m(\sigma_{pq})} (\bar{u}_p^n - \bar{u}_q^n) = \frac{m(p)}{k} \bar{u}_p^{n-1}, \tag{11}$$

starting with a given discrete image

$$\bar{u}_p^0 = \frac{1}{m(p)} \int_p u^0(x) dx, \quad p \in \mathcal{T}_h, \tag{12}$$

which is understood to be a piecewise constant approximation of a continuous image intensity  $u^0$ .

In (11),

$$g_{pq}^{\sigma, n-1} = g(|\nabla G_\sigma * \tilde{u}_{h,k}(x_{pq}, t_{n-1})|), \tag{13}$$

where  $\tilde{u}_{h,k}$  is an extension by 0 outside of  $\Omega$  of the piecewise constant function  $\bar{u}_{h,k}$  defined as follows

$$\bar{u}_{h,k}(x, t) = \sum_{n=0}^N \sum_{p \in \mathcal{T}_h} \bar{u}_p^n \chi_{\{x \in p\}} \chi_{\{t_{n-1} < t \leq t_n\}}, \tag{14}$$

with the Boolean function

$$\chi_{\{A\}} = \begin{cases} 1 & \text{if } A \text{ is true,} \\ 0 & \text{otherwise.} \end{cases}$$

We now restrict our attention to the specific situation depicted in Fig. 3 and derive coefficients of the scheme for the 3D cylindrical case. Define indices  $i = 1, \dots, n_1, j = 1, \dots, n_2, k = 1, \dots, n_3$  in radial, angular and vertical directions of the cylindrical coordinate system. In our case  $n_1 = m/2, n_2 = 2l, n_3 = n$ , and we define  $h_1 = 1/n_1, h_2 = 2\pi/n_2, h_3 = 1/n_3$ . The measure of the finite volume  $p$  corresponding to the triple  $(i, j, k)$  is given by  $m(p) = m_{ijk} = ((2i - 1)/2)h_1^2 h_2 h_3$ . Let  $\bar{u}_{ijk}^n$ , for the moment, denote the corresponding value  $\bar{u}_p^n$ . We define  $W_{ijk}, E_{ijk}, S_{ijk}, N_{ijk}, B_{ijk}, T_{ijk}$  using the transmission coefficients  $g_{pq}^{\sigma, n-1}(m(e_{pq})/m(\sigma_{pq}))$  at the sides of the finite volume  $p = (i, j, k), i = 1, \dots, n_1, j = 1, \dots, n_2, k = 1, \dots, n_3$  by

$$\begin{aligned} W_{ijk} &= g_{pq}^{\sigma, n-1}(i - 1)h_2 h_3, & q &= (i - 1, j, k), \\ E_{ijk} &= g_{pq}^{\sigma, n-1}i h_2 h_3, & E_{n_1jk} &= 0, \\ S_{ijk} &= g_{pq}^{\sigma, n-1} \frac{h_3}{\frac{2i-1}{2}h_2}, & q &= (i, j - 1, k), \\ N_{ijk} &= g_{pq}^{\sigma, n-1} \frac{h_3}{\frac{2i-1}{2}h_2}, & q &= (i, j + 1, k), \\ B_{ijk} &= g_{pq}^{\sigma, n-1} \frac{2i-1}{2} \frac{h_1^2 h_2}{h_3}, & q &= (i, j, k - 1), \\ T_{ijk} &= g_{pq}^{\sigma, n-1} \frac{2i-1}{2} \frac{h_1^2 h_2}{h_3}, & q &= (i, j, k + 1). \end{aligned} \tag{15}$$

We also introduce diagonal coefficients  $C_{ijk}$  and right-hand sides  $F_{ijk}$

$$C_{ijk} = \frac{m_{ijk}}{k} + W_{ijk} + E_{ijk} + S_{ijk} + N_{ijk} + B_{ijk} + T_{ijk},$$

$$F_{ijk} = \frac{m_{ijk}}{k} \bar{u}_{ijk}^{n-1}. \tag{16}$$

Finally, with these definitions we can write one row of the linear system (11) in the form

$$C_{ijk} \bar{u}_{ijk}^n - W_{ijk} \bar{u}_{i-1jk}^n - E_{ijk} \bar{u}_{i+1jk}^n - S_{ijk} \bar{u}_{ij-1k}^n - N_{ijk} \bar{u}_{ij+1k}^n - B_{ijk} \bar{u}_{ijk-1}^n - T_{ijk} \bar{u}_{ijk+1}^n = F_{ijk}.$$

It is easy that  $L_\infty$ -stability property

$$\min_{p \in \mathcal{I}_h} \bar{u}_p^0 \leq \min_{p \in \mathcal{I}_h} \bar{u}_p^n \leq \max_{p \in \mathcal{I}_h} \bar{u}_p^n \leq \max_{p \in \mathcal{I}_h} \bar{u}_p^0, \quad 1 \leq n \leq N, \tag{17}$$

can be shown. This property is important in image processing [20]. In order to show (17), we express scheme (11) in the form

$$\bar{u}_p^n + \frac{k}{m(p)} \sum_{q \in N(p)} g_{pq}^{\sigma, n-1} \frac{m(e_{pq})}{m(\sigma_{pq})} (\bar{u}_p^n - \bar{u}_q^n) = \bar{u}_p^{n-1}. \tag{18}$$

Let  $\max_{r \in \mathcal{I}_h} \bar{u}_r^n$  be achieved at the node  $p$ . Then the second term on the left-hand side of (18) is nonnegative and thus  $\bar{u}_p^n \leq \bar{u}_p^{n-1} \leq \max_{r \in \mathcal{I}_h} \bar{u}_r^{n-1}$ , which gives the result for max. The relation for min is derived in a similar way. The structure of (11) shows that the matrix of the system is a symmetric, diagonally dominant  $M$ -matrix. Therefore, the system has a unique solution and preconditioned iterative linear solvers [18] or additive operator splitting schemes [20] can be used efficiently.

**Remark.** Using the Gauss function  $G_\sigma = G_\sigma(x) = \frac{1}{(2\sqrt{\pi\sigma})^N} e^{-|x|^2/4\sigma}$  as the smoothing kernel, one can replace the term  $G_\sigma * u^{n-1}$  by solving the linear heat equation for time  $\sigma$  with the initial condition given by  $u^{n-1}$ . This linear equation can be solved numerically at the same 3D cylindrical grid by one implicit step with length  $\sigma$  (the only difference is that  $g_{pq}^{\sigma, n-1} \equiv 1$  in all above coefficients). Using that result we evaluate approximately  $g_{pq}^{\sigma, n-1}$  in points  $x_{pq}$  and use these values in (11).

**2.1. Definition.** A weak solution of the regularized Perona-Malik problem (1)–(3) is a function  $u \in L_2(I, V)$ , where  $V$  is the Sobolev space  $H^1(\Omega)$ , satisfying the identity

$$\int_0^T \int_\Omega u \frac{\partial \varphi}{\partial t}(x, t) \, dx \, dt + \int_\Omega u_0(x) \varphi(x, 0) \, dx - \int_0^T \int_\Omega g(|\nabla G_\sigma * u|) \nabla u \nabla \varphi \, dx \, dt = 0 \tag{19}$$

for all  $\varphi \in \Psi$ , there  $\Psi$  is the space of smooth test functions

$$\Psi = \{ \varphi \in C^{2,1}(\bar{\Omega} \times [0, T]), \nabla \varphi \cdot \vec{n} = 0 \text{ on } \partial\Omega \times (0, T), \varphi(\cdot, T) = 0 \}. \tag{20}$$

**2.2. Theorem.** The sequence  $\bar{u}_{h,k}$  given by scheme (11) converges strongly in  $L_2(Q_T)$  to the unique weak solution  $u$  of (1)–(3) as  $h, k \rightarrow 0$ .

**Proof.** We follow the convergence proof in [13] and outline only modification required for the cylindrical case. The structure of scheme (11) is the same as in [13]. Therefore, we get a priori

estimates of the discrete solutions, which are fundamental for the convergence proof. Thus, there is a positive constant  $C$ , independent of  $h$  and  $k$ , such that

- (i)  $\max_{0 \leq n \leq N} \sum_{p \in \mathcal{T}_h} (\bar{u}_p^n)^2 m(p) \leq C,$
- (ii)  $\sum_{n=1}^N k \sum_{(p,q) \in \mathcal{E}} \frac{m(e_{pq})}{m(\sigma_{pq})} (\bar{u}_p^n - \bar{u}_q^n)^2 \leq C.$

Differently from [13], we do not work with polygonal but curvilinear finite volumes. We must take this fact into account. Let  $\xi \in \mathbb{R}^d$  be a given vector. For all  $(p, q) \in \mathcal{E}$ , let  $\xi_{pq}(x) = \xi/|\xi| \cdot n_{pq}(x)$ . For all  $x \in \Omega_\xi = \{x \in \Omega, [x, x + \xi] \in \Omega\}$ , we let the function  $E(x, p, q)$  be defined by

$$E(x, p, q) = \begin{cases} 1 & \text{if the segment } [x, x + \xi] \text{ intersects in a point } y_{pq} \text{ interface } e_{pq}, \\ & \text{and } q, \text{ and } \xi_{pq}(y_{pq}) > 0, \\ 0 & \text{otherwise.} \end{cases}$$

For any  $t \in (0, T)$  there exists  $n \in \mathbb{N}$ , such that  $(n - 1)k < t \leq nk$ . Then for almost all  $x \in \Omega_\xi$ , we can see that

$$\bar{u}_{h,k}(x + \xi, t) - \bar{u}_{h,k}(x, t) = \bar{u}_{p(x+\xi)}^n - \bar{u}_{p(x)}^n = \sum_{(p,q) \in \mathcal{E}} E(x, p, q) (\bar{u}_q^n - \bar{u}_p^n),$$

where  $p(x) \in \mathcal{T}_h$  and  $x \in p$ . By the Cauchy-Schwarz inequality, we obtain

$$\begin{aligned} & (\bar{u}_{h,k}(x + \xi, t) - \bar{u}_{h,k}(x, t))^2 \\ & \leq \left( \sum_{(p,q) \in \mathcal{E}} E(x, p, q) \xi_{pq}(x_{pq}) m(\sigma_{pq}) \right) \left( \sum_{(p,q) \in \mathcal{E}} E(x, p, q) \frac{(\bar{u}_q^n - \bar{u}_p^n)^2}{\xi_{pq}(x_{pq}) m(\sigma_{pq})} \right). \end{aligned} \tag{21}$$

Geometrical arguments show that  $\xi_{pq}(x_{pq}) m(\sigma_{pq}) = \xi/|\xi| \cdot n_{pq}(x_{pq}) m(\sigma_{pq}) = c \xi/|\xi| \cdot (x_q - x_p)$ , where  $c = 1$  if  $\sigma_{pq}$  is a straight line and  $c = (\pi/n_2)/\sin(\frac{\pi}{n_2})$  if  $\sigma_{pq}$  is an arc. Since we have always at least two intersecting slices in the grid,  $n_2 \geq 4$  and  $c \leq \pi/2\sqrt{2} = C$ . Then again by the Cauchy-Schwarz inequality

$$\sum_{(p,q) \in \mathcal{E}} E(x, p, q) \xi_{pq}(x_{pq}) m(\sigma_{pq}) \leq C \frac{\xi}{|\xi|} \cdot (x_{p(x+\xi)} - x_{p(x)}) \leq C |x_{p(x+\xi)} - x_{p(x)}| \leq C(2h + |\xi|).$$

Now, we integrate relation (21) on  $\Omega_\xi \times (0, T)$

$$\begin{aligned} & \int_{\Omega_\xi \times (0, T)} (\bar{u}_{h,k}(x + \xi, t) - \bar{u}_{h,k}(x, t))^2 dx dt \\ & \leq C(2h + |\xi|) \sum_{n=1}^N k \sum_{(p,q) \in \mathcal{E}} \frac{(\bar{u}_q^n - \bar{u}_p^n)^2}{\xi_{pq}(x_{pq}) m(\sigma_{pq})} \int_{\Omega_\xi} E(x, p, q) dx, \end{aligned} \tag{22}$$

and again by the geometrical argument

$$\int_{\Omega_\xi} E(x, p, q) dx \leq m(e_{pq}) \xi_{pq}(x_{pq}) = m(e_{pq}) \frac{\xi}{|\xi|} \cdot n_{pq}(x_{pq}) |\xi| = m(e_{pq}) |\xi| \xi_{pq}(x_{pq}),$$

we obtain

$$\begin{aligned} & \int_{\Omega_\xi \times (0,T)} (\bar{u}_{h,k}(x + \xi, t) - \bar{u}_{h,k}(x, t))^2 dx dt \\ & \leq C(2h + |\xi|)|\xi| \sum_{n=1}^N k \sum_{(p,q) \in \mathcal{E}} \frac{m(e_{pq})}{m(\sigma_{pq})} (\bar{u}_q^n - \bar{u}_p^n)^2. \end{aligned} \tag{23}$$

Finally, using the a priori estimate (ii) we find that for any vector  $\xi \in \mathbb{R}^d$  there is a positive constant  $C$ , such that

$$\int_{\Omega_\xi \times (0,T)} (\bar{u}_{h,k}(x + \xi, t) - \bar{u}_{h,k}(x, t))^2 dx dt \leq C|\xi|(|\xi| + 2h). \tag{24}$$

Inequality (24) is called the *space translate estimate* in the finite volume methods. In the same way as in [13], we obtain the *time translate estimate*, i.e., there is a positive constant  $C$ , such that for all  $s \in (0, T)$ ,

$$\int_{\Omega \times (0,T-s)} (\bar{u}_{h,k}(x, t + s) - \bar{u}_{h,k}(x, t))^2 dx dt \leq Cs. \tag{25}$$

Using extension by 0 of  $\bar{u}_{h,k}$  outside  $\Omega$  and the *discrete trace inequality* (see [6,13]), we can extend (24) in the following way:

$$\int_{\Omega \times (0,T)} (\bar{u}_{h,k}(x + \xi, t) - \bar{u}_{h,k}(x, t))^2 dx dt \leq C|\xi|. \tag{26}$$

Estimates (26) and (25) are sufficient to use following well-known *Kolmogorov’s relative compactness criterion in  $L_2(Q_T)$*  (see e.g. [12]):

The set  $K \subset L_2(Q_T)$  is relatively compact if and only if

- (i)  $K$  is bounded, i.e., there exists a constant  $C > 0$  such that  $\|f\| \leq C$  for every  $f \in K$ ;
- (ii)  $K$  is mean equicontinuous, i.e., for every  $\varepsilon > 0$ , there exists  $\delta > 0$ , such that

$$\int_{Q_T} (f(x + \gamma) - f(x))^2 dx < \varepsilon^2$$

for each  $f \in K$  and  $\gamma$  with  $|\gamma| < \delta$ .

Since

$$\begin{aligned} & \int_{Q_T} (\bar{u}_{h,k}(x + \xi, t + s) - \bar{u}_{h,k}(x, t))^2 dx dt \\ & \leq 2 \int_{Q_T} (\bar{u}_{h,k}(x + \xi, t + s) - \bar{u}_{h,k}(x, t + s))^2 dx dt + 2 \int_{Q_T} (\bar{u}_{h,k}(x, t + s) - \bar{u}_{h,k}(x, t))^2 dx dt \end{aligned}$$

using a priori estimate (i) and estimates (26) and (25), by the Kolmogorov compactness criterion, we have that there exists function  $u \in L_2(Q_T)$  such that for some subsequence of  $\bar{u}_{h,k}$

$$\bar{u}_{h,k} \rightarrow u \quad \text{in } L_2(Q_T) \text{ as } h, k \rightarrow 0.$$

Moreover, using (24) we find that this limit function is in  $L_2(I, V)$  [6]. Therefore,  $u$  is a good candidate to be a weak solution of (1)–(3). To show that this is the case, let  $\varphi \in C_0^\infty(Q_T)$ ,  $\varepsilon > 0$  and  $\varphi(x, t) = 0$  if  $|x - \partial\Omega| < \varepsilon$ . Let  $0 < |\xi| < \varepsilon$ . Then by the Cauchy-Schwarz inequality

$$\int_{\Omega \times (0, T)} \frac{\bar{u}_{h,k}(x + \xi, t) - \bar{u}_{h,k}(x, t)}{|\xi|} \varphi(x, t) \, dx \, dt \leq \frac{\sqrt{C|\xi|(|\xi| + h)}}{|\xi|} \|\varphi\|_{L_2(Q_T)}.$$

For the limit function  $u$  we have

$$\int_{\Omega \times (0, T)} \frac{u(x + \xi, t) - u(x, t)}{|\xi|} \varphi(x, t) \, dx \, dt \leq \sqrt{C} \|\varphi\|_{L_2(Q_T)}.$$

On the other hand, by a changing of the variables  $y = x + \xi$ , we get

$$\begin{aligned} & \int_{\Omega \times (0, T)} \frac{u(x + \xi, t) - u(x, t)}{|\xi|} \varphi(x, t) \, dx \, dt \\ &= \int_{\Omega \times (0, T)} \frac{u(y, t)}{|\xi|} \varphi(y - \xi, t) \, dy \, dt - \int_{\Omega \times (0, T)} \frac{u(y, t)}{|\xi|} \varphi(y, t) \, dy \, dt \\ &= - \int_{\Omega \times (0, T)} \frac{\varphi(y, t) - \varphi(y - \xi, t)}{|\xi|} u(y, t) \, dy \, dt \\ &\leq C \|\varphi\|_{L_2(Q_T)}. \end{aligned} \tag{27}$$

Let  $\xi = \omega e_i$ , where  $e_i$  is  $i$ th coordinate vector, and let  $\omega \rightarrow 0$ . Then

$$- \int_{\Omega \times (0, T)} \frac{\partial \varphi(x, t)}{\partial x_i} u(x, t) \, dx \, dt \leq C \|\varphi\|_{L_2(Q_T)}, \quad \forall \varphi \in C_0^\infty(Q_T).$$

Thus  $u$  has generalized spatial derivatives in  $L_2(Q_T)$ , so it is in  $L_2(I, V)$ .

The last step is to prove that  $u$  fulfills the weak identity (19) from Definition 2.1, and thus it is a weak solution of the regularized Perona-Malik problem. Since such a solution is unique due to [4], not only a subsequence of  $\bar{u}_{h,k}$  but the whole sequence will converge to  $u$ . To show convergence, we follow discussion of [13], Section 3.3, with particular attention to only one step, which is different in cylindrical case. In [13, proof of Lemma 3.8], we should get an estimate

$$J = \left| \frac{\varphi(x_q, t_n) - \varphi(x_p, t_n)}{m(\sigma_{pq})} - \nabla \varphi(x_{pq}, t_n) \cdot n_{pq}(x_{pq}) \right| \leq Ch \tag{28}$$

for any smooth function  $\varphi \in \Psi$ . It is clearly true when  $\sigma_{pq}$  is a straight line, so we only consider the case when  $\sigma_{pq}$  is an arc. Then

$$\int_{\sigma_{pq}} \frac{\partial \varphi}{\partial T} \, ds = \varphi(x_q) - \varphi(x_p),$$

where  $T$  is the unit tangent vector to the curve  $\sigma_{pq}$ . By the mean-value theorem, there is a point  $\eta \in \sigma_{pq}$ , such that

$$\nabla \varphi(\eta) \cdot T(\eta) = \frac{\varphi(x_q, t_n) - \varphi(x_p, t_n)}{m(\sigma_{pq})}.$$

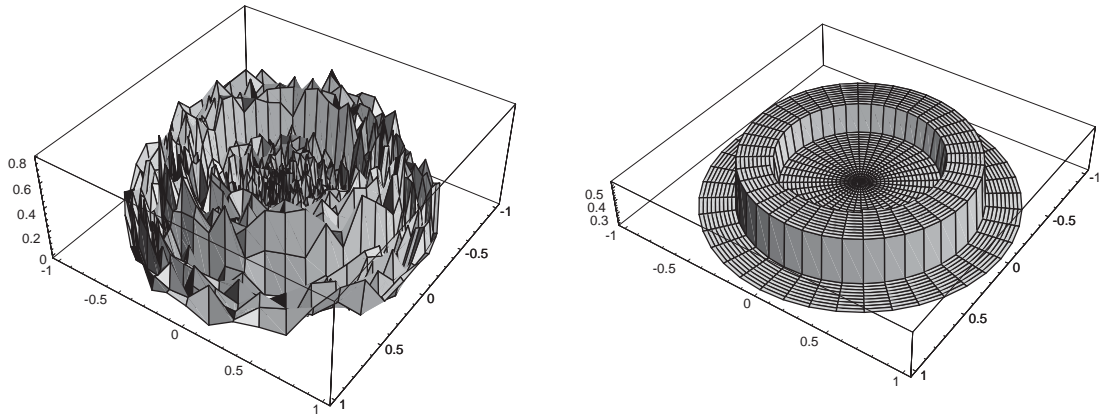


Fig. 4. Horizontal cut of artificially given noisy initial data (left) and its perfect reconstruction (right).

Since  $T(x_{pq}) = n_{pq}(x_{pq})$ , we have

$$\begin{aligned}
 J &= \left| \frac{\varphi(x_q, t_n) - \varphi(x_p, t_n)}{m(\sigma_{pq})} - \nabla\varphi(\eta) \cdot T(\eta) + \nabla\varphi(\eta) \cdot T(\eta) - \nabla\varphi(x_{pq}) \cdot T(x_{pq}) \right| \\
 &= |\nabla\varphi(\eta) \cdot (T(\eta) - T(x_{pq})) + (\nabla\varphi(\eta) - \nabla\varphi(x_{pq})) \cdot T(x_{pq})| \\
 &\leq |\nabla\varphi(\eta)| |T(\eta) - T(x_{pq})| + |\nabla\varphi(\eta) - \nabla\varphi(x_{pq})| |T(x_{pq})| \leq Ch
 \end{aligned}$$

due to the smoothness of  $\varphi$  and the fact that  $|T(\eta) - T(x_{pq})| \leq \pi/h_2 \leq Ch$  for any  $\eta \in \sigma_{pq}$ .  $\square$

### 3. Numerical experiments

In the first experiment, we consider an artificial example, in which the double valued radially symmetric intensity function is perturbed by additive noise. The initial noisy function and the result after application of 100 scale steps of scheme (11) is shown in Fig. 4. The reconstructed image perfectly corresponds to original data. We use the function

$$g(s) = \frac{1}{1 + Ks^2} \tag{29}$$

with  $K = 2$ .

Next we applied the method to real 3D cylindrical echocardiographic images given by 60 rotating slices with  $240 \times 200$  pixels. We have  $n_1 = 120$ ,  $n_2 = 120$  and  $n_3 = 200$ . One can see in Fig. 5, which displays a horizontal 2D cut of data in the center of cylinder (front view (left) and top view (right)), how noisy the original data is. Fig. 6 shows results after 2 and 10 steps of the algorithm with  $K = 1$ . In order not to conserve undesirable edges (speckle noise) a smaller value of  $K$ ,  $K = 0.1$ , is used for the diffusivity in the angular direction. Results are shown in Fig. 7 after the same number of scale steps.

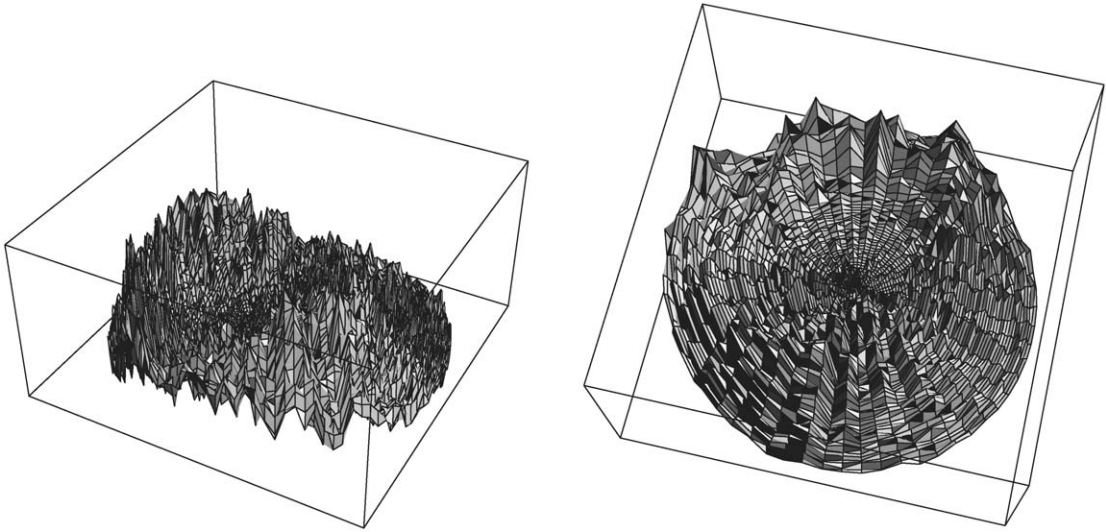


Fig. 5. Horizontal cut of 3D cylindrical echocardiographic data, front view (left), top view (right).

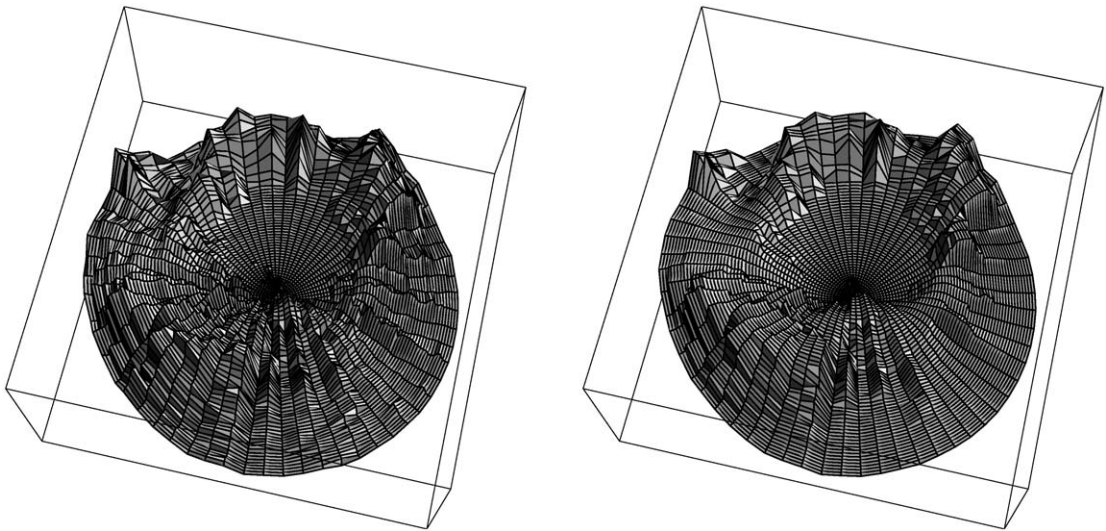


Fig. 6. Smoothing of the data after 2 (left) and 10 (right) scale steps of the algorithm.

In Fig. 8 we show visualization of the ventricular volume using original noisy data (left) and data after nonlinear smoothing by our algorithm (right). One can clearly see necessity of nonlinear filtering, to gain an understanding of the 3D ventricular shape.

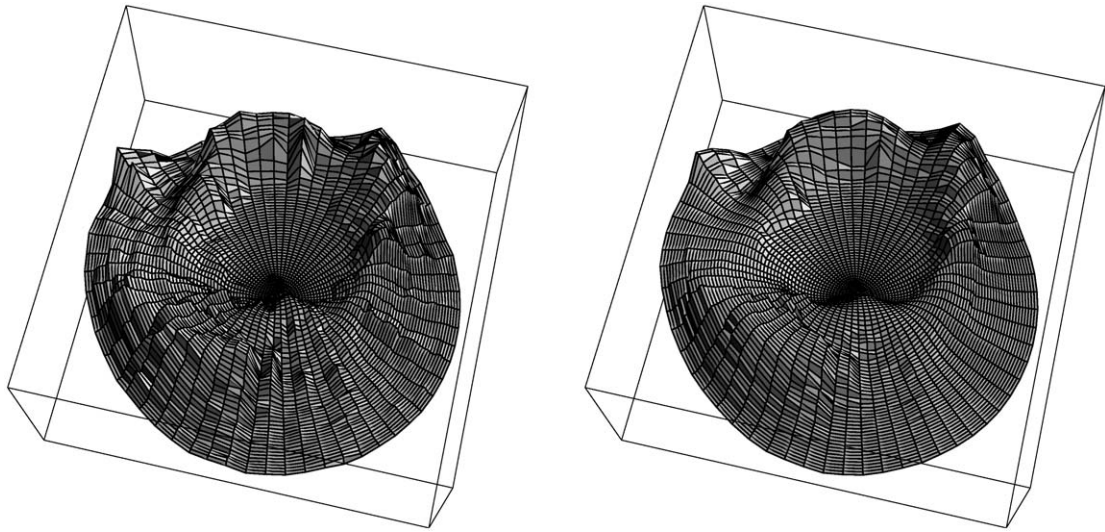


Fig. 7. Smoothing of the data after 2 (left) and 10 (right) scale steps of the algorithm with stronger diffusion in angular direction.

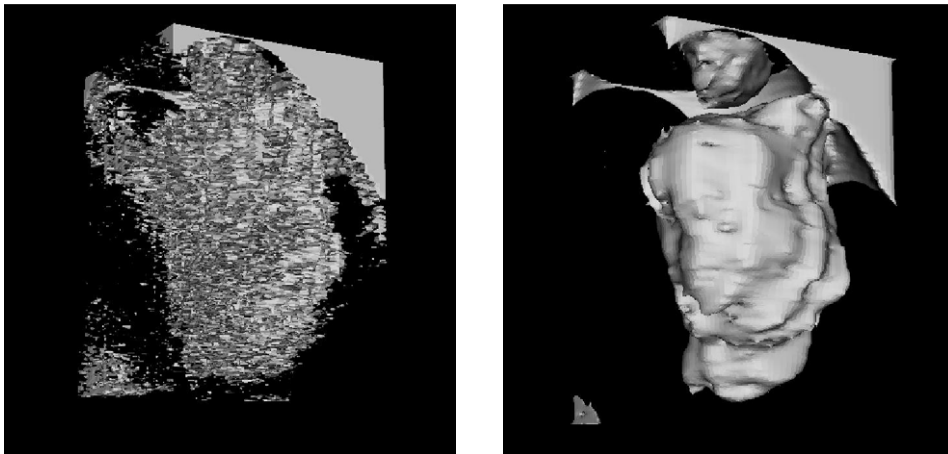


Fig. 8. Ventricular boundary visualized before (left) and after (right) nonlinear image smoothing.

### **Acknowledgements**

The authors gratefully acknowledge ESAOTE Biomedica, Firenze, Italy, for bringing the problem to their attention and providing 3D cylindrical echocardiographic images. The work was supported by NATO Grant PST.CLG.979123, by VEGA Grant 1/0313/03 and by Italian MIUR-Cofin 2002013422.

## References

- [1] L. Alvarez, F. Guichard, P.L. Lions, J.-M. Morel, Axioms and fundamental equations of image processing, *Arch. Rational Mech. Anal.* 123 (1993) 200–257.
- [2] H.N. Cardinal, J.D. Gill, A. Fenster, Analysis of geometrical distortion and statistical variance in length, area and volume in a linearly scanned 3D ultrasound image, *IEEE Trans. Med. Imaging* 19 (2000) 632–651.
- [3] F. Catté, P.L. Lions, J.-M. Morel, T. Coll, Image selective smoothing and edge detection by nonlinear diffusion, *SIAM J. Numer. Anal.* 29 (1992) 182–193.
- [4] G.H. Cottet, L. Germain, Image processing through reaction combined with non-linear diffusion, *Math. Comp.* 61 (1993) 659–673.
- [5] ESAOTE Biomedica, Firenze - private communications, 2000.
- [6] R. Eymard, T. Gallouet, R. Herbin, The finite volume method, in: Ph. Ciarlet, J.L. Lions (Eds.), *Handbook of Numerical Analysis*, Vol. 7, Elsevier, Amsterdam, 2000.
- [7] A. Fenster, D.B. Downey, 3-D ultrasound imaging: a review, *IEEE Eng. Med. Biol. Mag.* 15 (1996) 41–51.
- [8] A. Handlovičová, K. Mikula, F. Sgallari, Variational numerical methods for solving nonlinear diffusion equations arising in image processing, *J. Visual Comm. Image Represent.* 13 (2002) 217–237.
- [9] J. Kačur, K. Mikula, Solution of nonlinear diffusion appearing in image smoothing and edge detection, *Appl. Numer. Math.* 17 (1995) 47–59.
- [10] S. Kichenassamy, The Perona-Malik paradox, *SIAM J. Appl. Math.* 57 (1997) 1328–1342.
- [11] J.J. Koenderink, The structure of images, *Biol. Cybernet.* 50 (1984) 363–370.
- [12] A. Kufner, O. John, S. Fučík, *Function Spaces*, Academia, Prague, 1977.
- [13] K. Mikula, N. Ramarosy, Semi-implicit finite volume scheme for solving nonlinear diffusion equations in image processing, *Numer. Math.* 89 (2001) 561–590.
- [14] J. Montagnat, M. Sermesant, H. Delingette, G. Malandain, N. Ayache, Anisotropic filtering for model-based segmentation of 4D cylindrical echocardiographic images, *Pattern Recognition Lett.* 24 (2003) 815–828.
- [15] M. Nitzberg, T. Shiota, Nonlinear image filtering with edge and corner enhancement, *IEEE Trans. Pattern Anal. Mach. Intell.* 14 (1992) 826–833.
- [16] S.V. Patankar, *Numerical Heat Transfer and Fluid Flow*, Hemisphere, Washington, 1980.
- [17] P. Perona, J. Malik, Scale space and edge detection using anisotropic diffusion, *IEEE Trans. Pattern Anal. Mach. Intell.* 12 (1990) 629–639.
- [18] Y. Saad, *Iterative Methods for Sparse Linear Systems*, PWS, Boston, 1996.
- [19] A. Sarti, K. Mikula, F. Sgallari, Nonlinear multiscale analysis of three-dimensional echocardiographic sequences, *IEEE Trans. Med. Imaging* 18 (1999) 453–466.
- [20] J. Weickert, *Anisotropic Diffusion in Computer Vision*, Teubner, Stuttgart, 1998.
- [21] J. Weickert, Anisotropic diffusion filters for image processing based quality control, in: A. Fasano, M. Primicerio (Eds.), *Proceedings of Seventh European Conference on Mathematics in Industry*, Teubner, Stuttgart, 1994, pp. 355–362.
- [22] R.T. Whitaker, S.M. Pizer, A multiscale approach to nonuniform diffusion, *CVGIP: Image Understand.* 57 (1993) 99–110.
- [23] A.P. Witkin, Scale-space filtering, *Proceedings of the Eighth International Conference on Artificial Intelligence*, Vol. 2, 1983, pp. 1019–1022.